Received: 15 January 2024 | Revised: 31 March 2024 | Accepted: 3 April 2024

DOI: 10.1002/aoc.7492

RESEARCH ARTICLE

Applied Organometallic Chemistry WILEY

Synthesis of NiO nanoparticles from *Paulownia tomentosa* plant extracts via a green synthesis method and antibacterial, antibiofilm and cytotoxicity applications

Güney Gürsoy[1] | **Zehra Çiçek**[2] | **Saniye Tekerek**[3] | **Esin Kiray**[4] | **Ayça Tanriverdi**[3] | **Esen Çakmak**[5]

[1]Department of Biophysics, Department of Basic Medical Sciences, Faculty of Medicine, Kırşehir Ahi Evran University, Kırşehir, Turkey

[2]Department of Physiology, Gülhane Faculty of Medicine, University of Health Sciences, Ankara, Turkey

[3]Department of Material Science and Engineering, Graduate School of Natural and Applied Sciences, Kahramanmaraş Sütcü Imam University, Kahramanmaraş, Turkey

[4]Department of Medical Services and Techniques, Medical Laboratory Techniques Program, Vocational School of Health Services, Kırşehir Ahi Evran University, Kırşehir, Turkey

[5]Department of Bioengineering and Sciences, Graduate School of Natural and Applied Sciences, Kahramanmaraş Sütcü Imam University, Kahramanmaras, Turkey

Correspondence
Güney Gürsoy, Department of Biophysics, Department of Basic Medical Sciences, Faculty of Medicine, Kırşehir Ahi Evran University, Kırşehir, Turkey.
Email: guneygursoy@ahievran.edu.tr

This study revealed the effective production of nickel oxide nanoparticles (NPs) using chelating agents derived from the leaves of *Paulownia tomentosa* plants and nickel (II) chloride hexahydrate ($NiCl_2{\cdot}6H_2O$) as the precursor. Nickel oxide NPs (NiO NPs) have been successfully prepared by a green synthesis method using extracts of *P. tomentosa* leaves in water. The morphology and crystallinity of the NPs were investigated via X-ray diffraction (XRD), scanning electron microscopy (SEM), UV–visible spectroscopy (UV–vis), energy-dispersive X-ray analysis (EDX), Fourier transform infrared spectroscopy (FT-IR) and thermogravimetric analysis (TGA). The formation behaviour of NiO NPs and the microstructural and physical properties of the resulting particles were studied. This study additionally investigated the antimicrobial, antibiofilm and cytotoxic effects of NiO NPs. Microstructurally uniform NiO NPs with a nanometre diameter were consistently produced using an eco-friendly processing approach and exhibited a visible-range transparency of 89%. The obtained SEM images confirmed the octahedral shape of the NPs. The NiO NPs acquired were found to have potent antimicrobial efficacy against all the other bacterial strains. As a result of their antibiofilm effects on pathogenic *Escherichia coli* and *Pseudomonas aeruginosa* bacteria, NiO NPs strongly inhibited these bacteria in a concentration-dependent manner. In the cytotoxicity study of NiO NPs, a decrease in cell viability was shown to occur depending on the concentration of the cell lines used.

KEYWORDS
antimicrobial, cytotoxicity, green synthesis, nanoparticles, nickel oxide

1 | INTRODUCTION

Nanotechnology, which combines many disciplines, such as physics, material science, chemistry, medicine and biotechnology, has become popular for many studies worldwide. Nanotechnology is basically concerned with the production, characterisation and application of nano-scale materials.[1,2] Nanoparticle (NP) production is a very

important element of nanotechnology. NPs are considered basic building blocks with different properties owing to their small dimensions and large surface area-to-volume ratio.[3] Due to their small size and diverse shapes, NPs exhibit different properties than their bulk counterparts with larger surface areas.[4] NPs are generally synthesised by physical and chemical methods, but these methods have many disadvantages.[5–7] Plants have been used in many different ways from past to present. In this process, plants mostly play a role in the prevention and treatment of diseases.[8] Green synthesis is a method that provides an alternative to other methods and overcomes the limitations of traditional methods. In the green synthesis method, microorganisms or extracts of various plant parts are used.[9] Synthesising metal NPs via plant extracts is cost-effective, making it a useful and affordable alternative for large-scale metal NP production.[10] NPs created through an environmentally friendly synthesis technique have advanced biomedical properties. Moreover, these materials are biodegradable and nontoxic, making them safe options for use.[11] Several studies have investigated the antioxidant and antibacterial properties of NiO NPs.[12] NiO NPs obtained from the stem of the *Berberis balochistanica* plant were evaluated for their antibacterial, cytotoxic, stimulant and antifungal activities.[13] In another study, *Sageretia thea* (Osbeck.) Leaf extracts were used to acquire NiO NPs, the antibacterial activities of the obtained NiO NPs were studied, and minimum inhibitory concentrations (MICs) were calculated.[14] Gold, silver and zinc oxide NPs obtained from different fruit extracts and leaves have been shown to have inhibitory effects on the gram-positive bacteria *Staphylococcus aureus* and *Bacillus subtilis*, as well as the gram-negative bacteria *Pseudomonas aeruginosa* and *Escherichia coli* and different fungal species.[15–17] Antimicrobial agents are typically used as a main strategy for treating infections caused by biofilms.[18] The various components of the biofilm structure contribute to the development of antimicrobial resistance, and microorganisms within the biofilm exhibit strong resistance to antimicrobial agents.[19] Therefore, new treatment strategies are needed to overcome bacterial resistance and eliminate biofilm-forming bacteria.

In the literature, the mechanical and physical properties of wood were examined. The bark and blossoms of the Paulownia tree are utilised in traditional Chinese medicine to treat inflammatory and infectious illnesses.[20,21] Additionally, it is acknowledged for its effectiveness in treating conditions such as haemorrhoids, traumatic bleeding, bacteriological diarrhoea, hypertension and dysentery.[22] The antimicrobial, antioxidant and cytotoxic effects of extracts of the flowers, petals, bark, leaves and wood parts of *P. tomentosa* were investigated. The results showed that the best antimicrobial activity was achieved by the extract of the flower part of *P. tomentosa* against *S. aureus*.[23] In studies on the leaves and flowers of *P. tomentosa*, antioxidant properties were analysed, and catechin was found to have the highest phenolic content. This plant species therefore has potential for use in phytotherapy, pharmacology, modern medicine and the animal feed industry.[24] Paulownia leaves were found to contain a compound called catechin. Catechin, a colourless compound, has become a natural antioxidant of great interest because of its antioxidant, anticarcinogenic and antiobesity properties. Considering these properties, it can be concluded that the leaves of the Paulownia plant are a rich source of antioxidants. Considering these findings, plants can be used for medicinal purposes in the fight against many diseases, especially cancer. Based on this information, it has been observed that Paulownia leaves possess characteristic features that can serve as a preservative in animal feed and beverages. In the Paulownia trees, the leaf extract exhibited a higher concentration of β-carotene (7716 μg/g). Carotenoids found in nature typically possess potent antioxidant activity. Furthermore, β-carotene has been shown to have multiple beneficial medical effects, including antioxidant, provitamin A and anticancer effects. The results indicated that the Paulownia tree possesses medicinal properties with antioxidant content that aligns with the content analysis.[25]

In the present study, NiO NPs were synthesised via the green synthesis method using *P. tomentosa* leaf extract. The synthesised NiO NPs were characterised structurally and morphologically using appropriate methods. After the characterisation process, the antimicrobial, antibiofilm and cytotoxic properties of the NiO NPs were investigated. In this study, NiO NPs were preferred because efficient results can be obtained through biological activities due to their large surface area. For this purpose, NiO NPs have the potential to be superior to other materials when produced by green synthesis; in this research, their potential as therapeutic agents was elucidated for the first time.

2 | MATERIALS AND METHODS

2.1 | Preparation of NiO NPs using an extract of *P. tomentosa*

Leaves of *P. tomentosa* plants were collected from parks and gardens in the Kahramanmaraş region. These Paulownia leaves were dried at 50°C for 24 h to remove all moisture. The dried leaves were ground using a grinder. The Paulownia leaves were pulverised into powder and stored in sterile glass. Approximately 2 g of the

herbal powder was mixed with 40 mL of distilled water at 45°C for 30 min. The aqueous extract was filtered with Whatman 1 filter paper, and the resulting solution was prepared. Nickel (II) chloride hexahydrate salts (Afg-Bioscience 399218-250G) (1.6 g) were slowly added to 50 mL of the herbal solution; at this point, a substantial colour change was observed. The solution was then stirred at 75°C for 24 h. After the reaction, the reduction of Ni2+ to Ni0 was observed by the change in colour from greenish to yellowish-brown, indicating the formation of nickel oxide NPs. After reducing the metal salts to NPs, the samples were centrifuged for another 15 min at room temperature (5000 rpm). The centrifuged powders were left to dry at room temperature, annealed at 400°C for 2 h to form pure nickel oxide NPs and stored at 4°C until further use. The experimental steps of NiO NPs prepared by green synthesis are shown schematically in Figure 1.

2.2 | Characterisation of NiO NPs

Characterisation measurements included analysing the particle shape, size distribution, degree of aggregation, surface charge and surface area. An X-ray diffractometer (XRD) (Philips X'Pert PRO, the Netherlands, Cu Kα radiation, wavelength 1.54Å, 2θ, 20° to 80°) was used to investigate the structural properties of the NPs obtained using green synthesis. A scanning electron microscopy (SEM) (EVO40-LEO, Carl Zeiss, UK) image was used to determine the surface morphology and microstructure of the NPs. A UV–vis spectrophotometer (PG-T60, PG Instruments Ltd., UK) was used to record the absorbance spectra of the film samples in the wavelength range of 650–1100 nm. Thermogravimetric analysis (TGA) was performed with a Perkin Elmer Pyris 1, whereas differential thermal analysis (DTA) was performed using a Perkin Elmer DSC 4000. Fourier transform infrared (FTIR) spectroscopy was carried out at wavelengths ranging from 4000 to 400 cm^{-1} (Perkin Elmer Spectrum 400, Shimadzu, Japan).

The grain sizes of the NPs were calculated using the data obtained from the XRD diffraction pattern and the Debye–Scherrer formula. According to the Debye–Scherrer formula, the relationship between the crystal size and the half-intensity width is given by the Equation 1.

$$D = \frac{0.9\lambda}{\beta cos\theta}. \quad (1)$$

Here, D is the crystal size, λ is the wavelength of the X-ray used (1.5418 A°A), β is the half-intensity peak width (FWHM) and θ is the Bragg angle.

FIGURE 1 Experimental process for NiO nanoparticles (NPs) produced by green synthesis.

2.3 | Determination of the antimicrobial activity of NiO NPs

The antimicrobial activity of NiO NPs synthesised by the green synthesis method was established by the agar well diffusion method on gram-negative and gram-positive bacteria. In the analysis, *E. coli* ATCC 25922, *Enterococcus faecalis* ATCC 29212, *Listeria monocytogenes* ATCC 19115, *Acinetobacter baumannii* ATCC 17978, *P. aeruginosa* ATCC 27853, *S. aureus* ATCC 25923, *Bacillus cereus* ATCC 14579, *Staphylococcus epidermidis* ATCC 12228, *Shigella dysentery* ATCC 13313, *Klebsiella pneumoniae* ATCC 13883 and *Enterobacter aerogenes ATCC* 13048 were used to determine the activity of the NPs. Pathogenic bacteria were cultured overnight on brain heart infusion agar (BHIA) (Merck, Germany). Then, 100 μL of NiO NPs was added to each well, and the samples were incubated at 37°C for 1 day. The experiments were performed in triplicate. Antimicrobial activity was determined by measuring the diameter of the inhibition zone (mm).

2.4 | Determination of the minimum inhibitor (MIC) concentration

The minimal inhibitory concentration (MIC) was determined using a modified standard of the Clinical and Laboratory Standards Institute (CLSI) liquid microdilution method. *E. coli* ATCC 25922, *E. faecalis* ATCC 29212, *L. monocytogenes* ATCC 19115, *A. baumannii* ATCC 17978, *P. aeruginosa* ATCC 27853, *S. aureus* ATCC 25923, *B. cereus* ATCC 14579, *S. epidermidis* ATCC 12228, *S. dysentery* ATCC 13313, *K. pneumoniae* ATCC 13883 and *E. aerogenes ATCC* 13048 were used. The MIC determination was performed in 96-well plates using tryptic soy broth (TSB) medium. After overnight incubation at 37°C, the cultures were diluted to 1×10^6 CFU/mL, and 50 μL of bacteria was inoculated into each well. NiO NPs were added to 50 μL of solution in 96-well plates at different concentrations (256–0.5 μg/mL). The plates were incubated at 37°C for 18 h. The minimum concentration without visible bacterial growth was defined as the MIC. Gentamicin (Sigma-Aldrich, USA), a broad-spectrum antibiotic, was used as a positive control.[26]

2.5 | Determination of the antibiofilm activity of NiO NPs

To determine the antibiofilm activity of NiO NPs obtained by the green synthesis method with *P. tomentosa*, biofilm-producing *E. coli* ATCC 25922 and *P. aeruginosa* ATCC 27853 strains were used. After serial dilutions, 100 mL of test compounds (0.625–10 mg/mL) and 100 mL of bacterial culture ($OD_{600} = 0.132$) activated in TSB medium at 37°C were transferred to 96-well polystyrene microtiter plates. After 24 h of incubation at 37°C, the cells adhering to the wells were carefully rinsed with distilled water and allowed to air dry. Staining was performed under aseptic conditions with 0.4% (w/v) crystal violet, followed by rinsing with distilled water. Ethanol (200 mL) was used to dissolve the crystal violet solution. TSB medium (100 mL) was used as a negative control, and compound-free bacterial cultures were used as a positive control. The absorbance of the wells was measured at 595 nm (BioTek Epoch 2 Microplate Spectrophotometer, USA). The antibiofilm activity (%) was determined by the following formula. The study was repeated three times. The study was repeated three times. The antibiofilm activity was determined by the is given by the Equation 2.

$$\text{Antibiofilm activity}\,(\%) = \left(1 - \text{OD}_{\text{sample}}/\text{OD}_{\text{control}}\right) \times 100. \quad (2)$$

2.6 | Cell culture cytotoxicity activity (MTT assay)

HT-22 and MCF-7 cells were placed in 96-well plates with 100 μL of the cell suspension at a density of 1×10^5 cells/mL per well and incubated for 24 h (HT-22; High glucose DMEM (Capricorn, Cat. No: DMEM-HA, Germany), MCF-7; RPMI (Capricorn, Cat. No:RPMI-A, Germany). After incubation, NiO NPs were applied to the cells at specified concentrations (0–500 μg/mL). After the application, the cells were again incubated for 24 h at 37°C in a 5% CO_2, 95% humidity environment. After the 24-h period, the chemical solution in the wells was removed, and 100 μL of fresh cell medium and 10 μL of MTT were added to each well and incubated for 4 h. After incubation, the MTT (Cayman, 21795, USA) solution was removed from the wells, 100 μL of DMSO (Dimethyl sulfoxide; Emplura, Merck, M1.16743.1000, Germany) was added, and the mixture was incubated for approximately half an hour. The absorbance (OD, optical density) at a wavelength of 570 nm was measured with a microplate reader (Eon, Biotec). In the experiments, the groups were studied in triplicate.

2.7 | Statistical analysis

The chi-square test was used for statistical analysis of all the descriptive statistics. The significance value was set as $p = 0.01$. The Statistical Package for Social Sciences

(SPSS) for Windows (Version 23.0; SPSS, Inc., Chicago, IL) was used for all analyses. The statistical analyses for the cytotoxicity studies were performed using GraphPad Prism 9. All the experiments were performed in triplicate, and the data are expressed as the mean ± standard deviation (mean ± SD). Control comparisons were made using one-way analysis of variance (ANOVA), and Tukey's test was used as a post hoc test. A p value < 0.001 was considered to indicate statistical significance.

3 | RESULTS AND DISCUSSION

3.1 | Characterisation

XRD was carried out to ascertain and explore the crystal structure of the NiO target materials. Finally, diffraction patterns were obtained at room temperature with a scan rate of 4°/min for NiO NP target materials between diffraction angles (2θ) of 20° and 90°. The crystal structure of the NiO NPs was analysed using an XRD, as illustrated in Figure 2. The Paulownia NiO NPs produced a foam cubic crystalline structure (a:b:c: 3.52400 Å; density = 8.91 g/cm^3). The XRD pattern analyses of the NiO NPs are given in Table 1 (JCPDS card no 3-065-2865). Using the Debye–Scherrer equation, the average crystal size of the films was calculated to be 29.64 nm.

The X-ray diffraction peaks at 37°, 43°, 62°, 76° and 79° confirm the presence of cubic nickel oxide on the (111), (200), (220), (311) and (222) lattice planes, respectively. In addition, Figure 2 displays the X-ray diffraction patterns of the NiO NPs within the 2θ range of 42°–45°. The obtained patterns correspond to JCPDS card no. 04-0835. The NiO peaks, including the primary characteristic peak at 43°, are distinguishably wider than the other peaks and exhibit sharper peaks that can be attributed to the lower crystalline structure of the particles with smaller grain sizes.[27,28] The particle size–density graph indicates that all the powders are polydisperse, with peaks present in multiple regions ranging from the nanometre scale to the submicron scale. The peak density of large particles is greater than that of small particles because large particles scatter much more light than smaller particles.[29]

The sample surface morphology of the powder target material was assessed using SEM at magnifications of 1×x and 10.00×x. Analysis of the images indicates that the particles exhibit a high degree of agglomeration. The NiO powder SEM images are shown in Figure 3. As shown in the SEM images, NPs were formed in the nanowire foam structure. Large particles are observed due to the collection and agglomeration of smaller particles. A uniform distribution of small, randomly distributed grains is evident, as are homogeneous spherical particles.[30]

A UV–vis spectrophotometer was used to determine the characteristic light absorption bands of the NiO NPs obtained from the Paulownia leaves (Figure 4). The absorption of NiO NPs synthesised with leaf extracts was determined at a wavelength of 322 nm (Figure 4a). The highest absorptance curves were exhibited in the absorbance spectra at a wavelength of approximately 302 nm. These herbal extract, which mostly absorbsance in the UV range.

The Paulownia extract transmittance data are displayed in Figure 4b, with 81.51% of the NPs at 500 nm and 81.51 89.44% at 700 nm. These spectra exhibit the

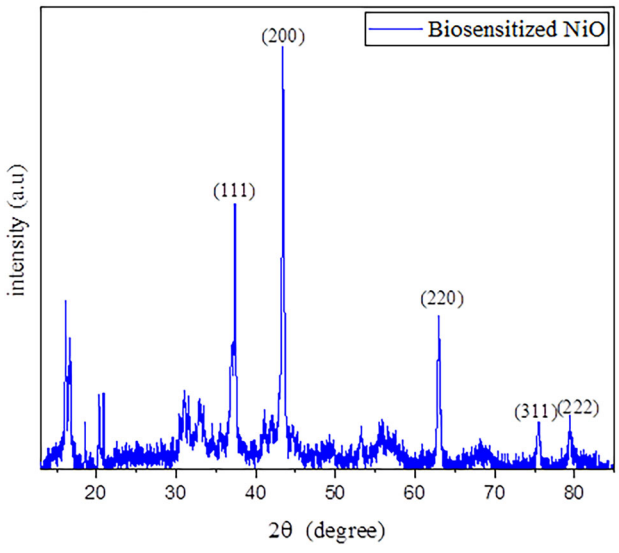

FIGURE 2 X-ray diffraction patterns of the biosynthesised NiO nanoparticles (NPs).

TABLE 1 Structural properties of Paulownia NiO NPs.

	Observed values				
Material	2θ (°)	FWHM	d (Å)	(hkl)	D (nm)
NiO	16.12	0.25619	5.49	(220)	31.31
	18.57	0.10536	4.77	(311)	76.40
	20.33	0.23848	4.36	(222)	33.84
	20.89	0.12571	4.24	(001)	64.26
	32.92	0.89978	2.71	(100)	9.20
	37.29	0.56054	2.40	(111)	14.95
	43.40	0.34870	2.08	(200)	24.52
	53.20	0.39620	1.72	(200)	20.20
	62.96	0.43487	1.48	(220)	21.42
	75.45	0.51919	1.26	(311)	19.34
	79.50	0.97012	1.20	(222)	10.65

Abbreviations: FWHM, half-intensity peak width; NPs, nanoparticles.

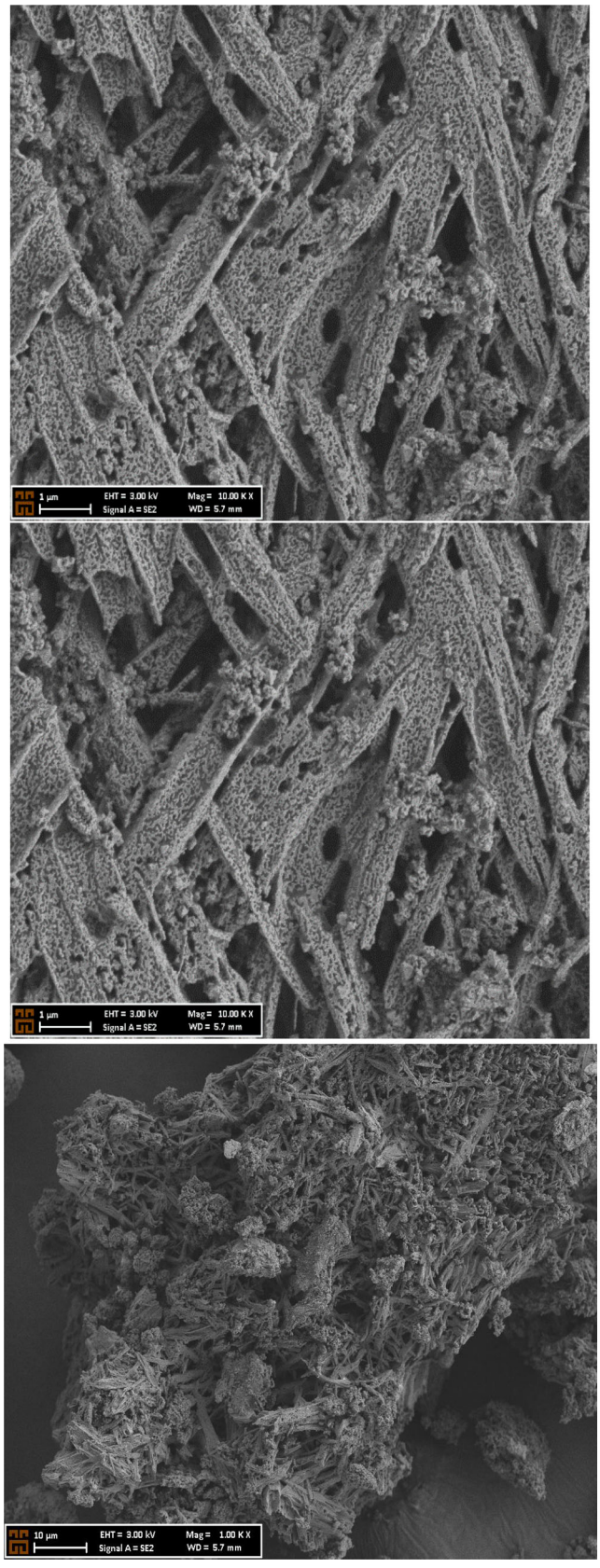

FIGURE 3 Scanning electron microscopy (SEM) micrograph of NiO nanopowders obtained after annealing at 450°C for 2 h.

characteristics of a Paulownia extract, which mostly trancmittance visible and infrared region range.

Fourier transform infrared spectroscopy (FTIR) was used to evaluate functional groups of reducing agents in water extract of Pauolownia (Figure 5a) and green synthesised NiO nanowire foam (Figure 5b) as shown in the Figure 5. The FTIR spectrum exhibited peaks between 1050 and 1300 cm^{-1} attributed to C–O bonds; between 1630 cm^{-1} attributed to C=O, C=C and C=N bonds; and between 3289 cm^{-1} assigned to O-H bonds (Figure 5a). The peak for NiO is observed at 743.8 cm^{-1} and corresponds to the stretching mode of the NiO NPs. The FTIR spectra of the NiO NPs show that the broad absorption bands at 3329 and 1621 cm^{-1} are assigned to O–H stretching and bending modes of water, respectively (Figure 5b). In the FT-IR spectrum of green synthesised NiO NPs, the broad band near 3329, 1621 cm^{-1} and 1233 cm^{-1} is due to the presence of effective biological reduction agents in the NiO NPs and is also assigned to the O–H stretching mode of the interlayer and adsorption water in Paulownia leaves extract (Figure 5b).[31,32] On the other hand, biological molecules may be involved in the stabilisation and reduction processes, which would explain the peaks' decreasing strength in the NiO NPs spectrum in comparison to the extract spectrum.

TGA was used to study the thermal characteristics of the NiO NPs. The typical TGA curve of the vanguard produce is shown in Figure 6. Weight loss clearly occurred in two temperature zones, 40–210°C and 456–737°C. The primary weight loss occurs between 40°C and 210°C, which is ascribed to the evaporation of the absorbed water. The second weight loss occurs between 456°C and 737°C, which can bind to the converted Ni(OH)2 to NiO. Above 737°C, the TG curve remains constant, indicating no change in the weight of the NPs. This information can guide the selection of calcination temperature. The total weight loss reached 40.08% at 737°C, and the weight loss occurred in two stages.

The DTA curve shows a wide endothermic response in the temperature range of 50–595°C, with an extensive peak occurring at 337°C. A large endotherm refers to the absorption of external heat to decompose a material. This is attributed to the release of energy that can be used for phase formation. The peak in the DTA curve implies that an event, such as combustion caused by impurities, has taken place within the structure. The $Ni(OH)_2$ structure changes to NiO between 50°C and 595°C, while the constant region above 595°C signifies the completion of the transformation to NiO.[33] The thermal dissociation and steadiness observed from the TGA-DTA curve can be strongly associated with the XRD data used for research

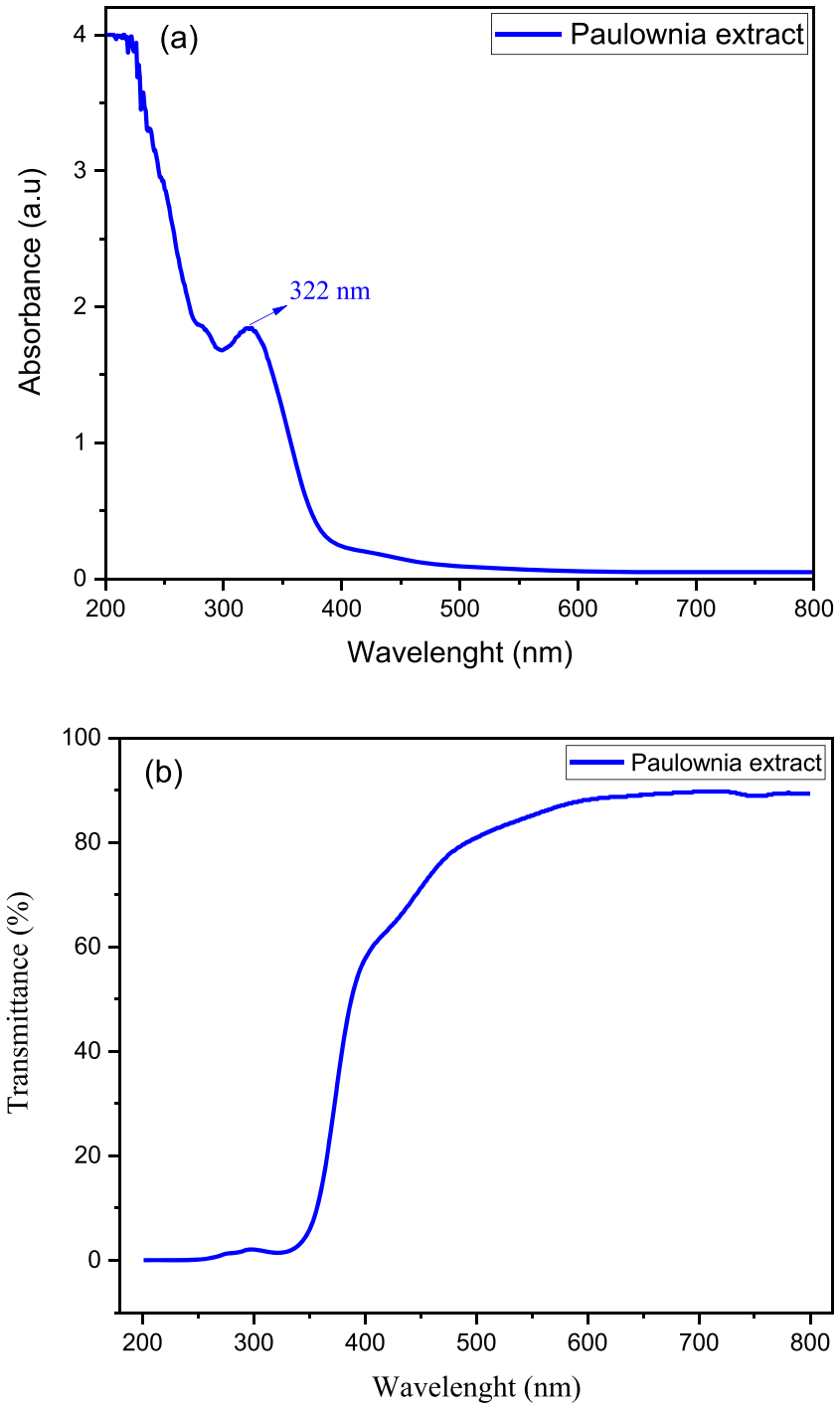

FIGURE 4 (a) Absorbance spectrum of Paulownia leaf extract and (b) UV–vis transmittance spectrum of the leaf extract.

on the phase transmutation of specimens tempered between 400°C and 700°C.

3.2 | Antimicrobial activity and MIC

The antibacterial activity of the newly synthesised Paulownia-mediated NiO NPs was evaluated against 11 different reference bacterial strains. The results obtained showed that the NiO NPs exhibited very strong antimicrobial activity and were effective against all the tested bacteria, as indicated in Table 2 (Figure 7). Notably, NiO NP complexes had low MICs for microorganisms. When the results of the compounds tested with gentamicin, which was used as a positive control in the present study, were compared, the MIC values were similar.

Gram-positive bacteria differ from Gram-negative bacteria in that they have a thick cell wall that is more porous and has higher permeability, and they do not

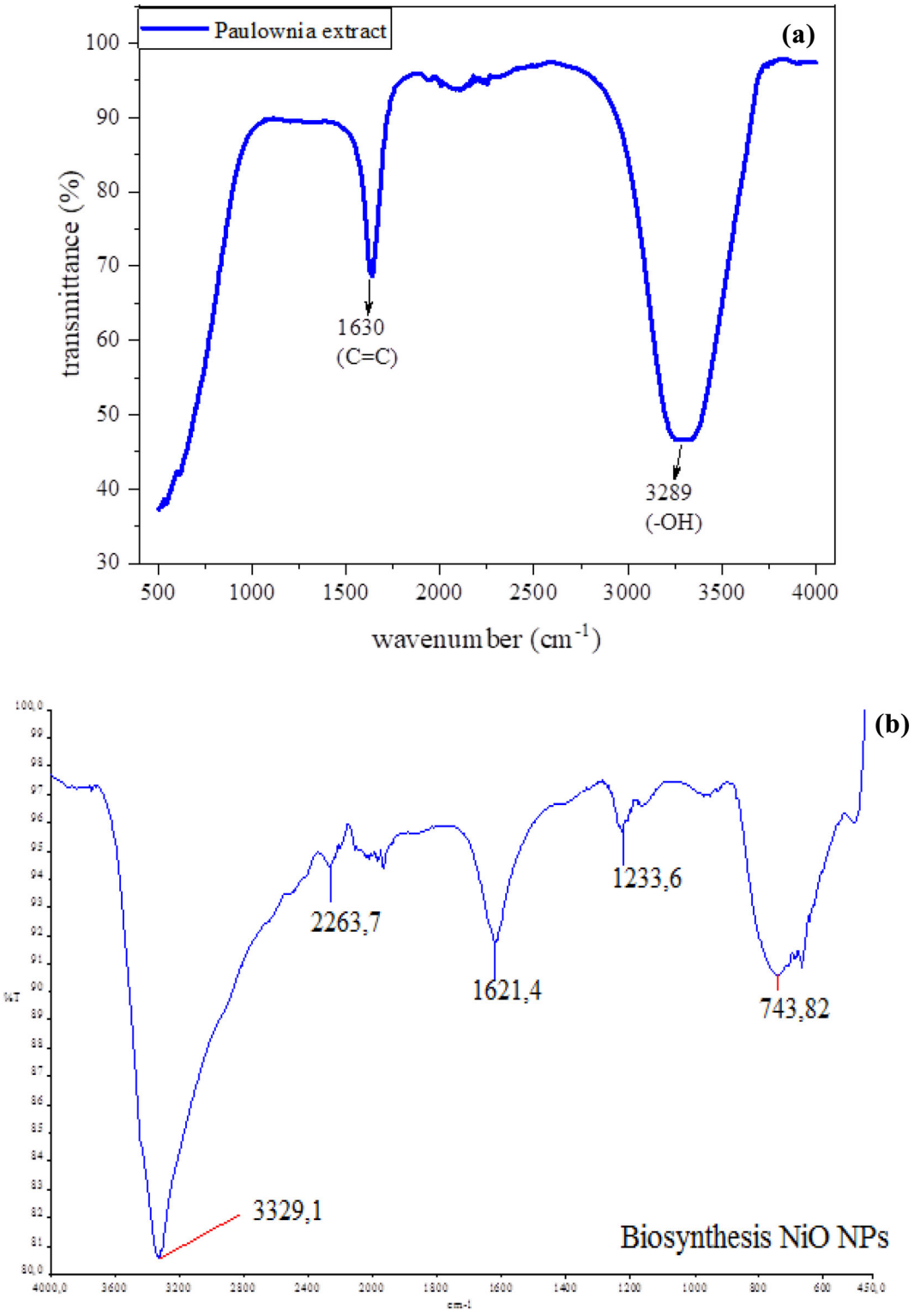

FIGURE 5 (a) Fourier transform infrared (FTIR) spectrum of Paulownia leaf extract and (b) FTIR spectrum showing the infrared vibrational modes of the biosynthesised NiO nanopowder.

have an outer lipid membrane. Gram-negative bacteria have a thin peptidoglycan layer and an outer lipid membrane. This difference in cell wall components results in different adhesion pathways for NPs. NiO NPs can adhere to both cell walls and membranes, which may affect their structure, transport activity and permeability. The nanoscale-sized outer cell membrane of bacteria results in good reactivity towards NPs. Because Gram-

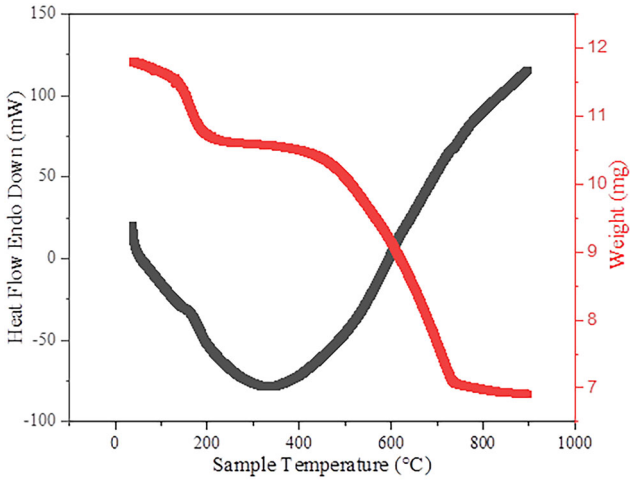

FIGURE 6 Thermogravimetric analysis (TG and differential thermal analysis [DTA]) curves of the NiO nanoparticles (NPs).

negative bacteria have thinner cell walls and less peptidoglycan, NiO NPs generally exhibit greater antibacterial activity against Gram-negative bacteria than Gram-positive bacteria.[34,35] In our study, its effectiveness on Gram-negative bacteria is given in Table 2.

The high antibacterial activity of NPs can be attributed to their size, morphology, chemical composition, ability to release metal ions for trans-membrane electron transfer, penetration, oxidation of cell organelles and production of some secondary products (reactive oxygen species, ROS), which cause cell damage. The antibacterial activities of NiO NPs may result from attractive electrostatic forces between the negatively charged cell membrane and positively charged Ni $^{2+}$ ions. Ni $^{2+}$ released from NiO NPs can penetrate the cell wall and damage DNA, mitochondria, protein and disrupt electron transport, resulting in cellular death.[35]

3.3 | Antibiofilm activity

The *E. coli* ATCC 25922 and *P. aeruginosa* ATCC 27853 strains were used to determine the antibiofilm activity of compounds containing NiO NPs. NiO NPs were found to have strong biofilm inhibitory effects on both types of strains, which increased with increasing concentration. At a concentration of 10 mg/mL, the NiO NP compound inhibited 64.27% of the *E. coli* ATCC 25922 strain biofilms and 72.14% of the *P. aeruginosa* ATCC 278533 strain biofilms (Figure 8). NiO NP compounds were found to have greater biofilm inhibitory effects on *P. aeruginosa*. Due to the strong antibacterial and antibiofilm activities of these newly synthesised compounds, they can be used as potential alternatives in both biomedical applications and industry.

3.4 | Cytotoxic activity

In Figure 9, cell viabilities in the mouse hippocampal neuronal cell line (HT-22) at different concentrations of NiO NPs are given as percentages compared with those in the control group. The study groups were as follows: a sham group (supplemented with ethanol at a dose of 500 μg/mL) and specified dose groups, with a minimum of 0.1 and a maximum of 500 μg/mL. Cell viability was found to be 92.82% in the sham group, based on the amount of ethanol used at a dose of 500 μg/mL. The small decrease in vitality was not statistically significant compared with that in the control group ($p > 0.05$). Cell viability showed a change between 99.16% and 92.46% at the doses of 0.1, 1 and 10 μg/mL chosen to determine the effect of low doses, but these partial changes were not significant compared to those in the control group ($p > 0.05$). At a concentration of 50 μg/mL, the cell viability exhibited a critical change and decreased to 75.80%. The change in viability at this dose was found to be significant compared to that in both the control group and the sham group (compared to the sham group; $p < 0.005$; compared with the control group; $p < 0.001$). The significant change in the sham group determined according to the high dose clearly demonstrated the effect of NiO NPs. With increasing concentrations, the effect of NiO NPs on cell viability became more evident, and the viability was 41.14% at 100 μg/mL and 9.82% at 500 μg/mL. In particular, concentrations above 100 μg/mL had toxic effects by causing a significant decrease in the viability of HT-22 cells (Figure 10). The dramatic decrease in viability was found to be statistically significant compared to that of the control and sham groups ($p < 0.001$). The concentration at which 50% of the cells were inhibited (IC_{50}) in HT-22 cells was determined to be 92.93 ± 2.6 μg/mL.

Figure 11 shows the effect of the determined doses of sham and NiO NPs on the viability of human breast cancer cells (MCF-7). The application groups for MCF-7 cells consisted of a sham treatment (the amount of ethanol applied at the maximum dose used for NiO NPs) and different doses of NiO NPs. As a result of the application in the sham group, cell viability was determined to be 88.66%. This decrease in viability was statistically significant compared with that of the control group ($p < 0.05$). On the other hand, low doses of NiO NPs (e.g., 0.1, 1 and 10 μg/mL) did not cause a significant change in cell viability ($p > 0.05$). After treatment with 50 μg/mL, the viability of the MCF-7 cells was 78.36%, but this decrease was significant ($p < 0.001$) compared with that of the control group but not significantly different from that of the sham group ($p > 0.05$). However, determining the activity of the NiO NPs was difficult. After treatment with

TABLE 2 Antimicrobial zone diameters of pathogenic strains affected by NiO NPs and compounds with different compositions.

	Antimicrobial zone diameter Gram-negative					
	***E. coli* ATCC 25922**	***P. aeruginosa* 27853**	***A. baumannii* ATCC 17978**	***K. pneumoniae* ATCC 13883**	***E. aerogenes* ATCC 13048**	***S. dysenteriae* ATCC 13313**
NiO NPs	21 ± 0.7	21 ± 1.4	22 ± 0.9	24 ± 0.7	23 ± 1.8	23 ± 0.4
MIC[a] (uM)						
NiO NPs	8	2	4	0.5	8	4
CN[b]	0.5	1	0.5	1	1	0.5

Abbreviations: MIC, minimum inhibitory concentrations; NPs, nanoparicles.
[a]Minimum inhibitory concentration (256–0.5 μg/mL) was determined as the lowest concentration inhibiting bacterial growth determined in three independent experiments performed in triplicate.
[b]CN: Gentemycin.

TABLE 2 (Continued)

	Antimicrobial zone diameter Gram pozitive				
	***S. aureus* 25923**	***B. cereus* ATCC 14,579**	***E. faecalis* ATCC 29,212**	***S. epidermidis* ATCC 12228**	***L. monocytogenes* ATCC 19115**
NiO NPs	23 ± 0.6	26 ± 1.3	20 ± 1.4	24 ± 1.4	30 ± 0.8
MIC[a] (uM)					
NiO NPs	8	2	4	4	0.5
CN[b]	0.5	1	0.5	0.5	0.5

Abbreviations: MIC, minimum inhibitory concentrations; NPs, nanoparicles.
[a]Minimum inhibitory concentration (256–0.5 μg/mL) was determined as the lowest concentration inhibiting bacterial growth determined in three independent experiments performed in triplicate.
[b]CN: Gentemycin.

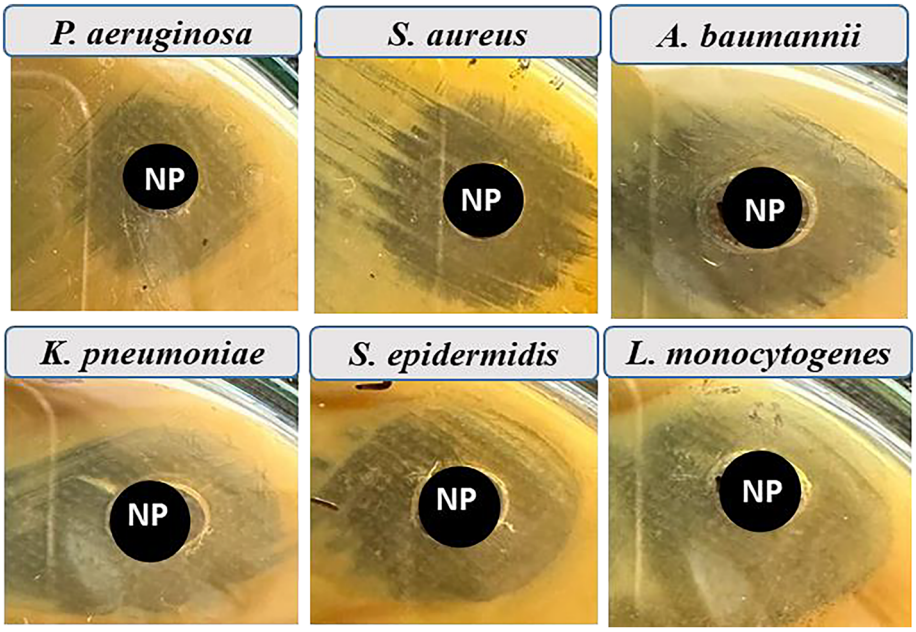

FIGURE 7 Inhibition zone diameters of green synthesised NiO nanoparticles (NPs, 256 μg/mL concentration) on various pathogenic strains.

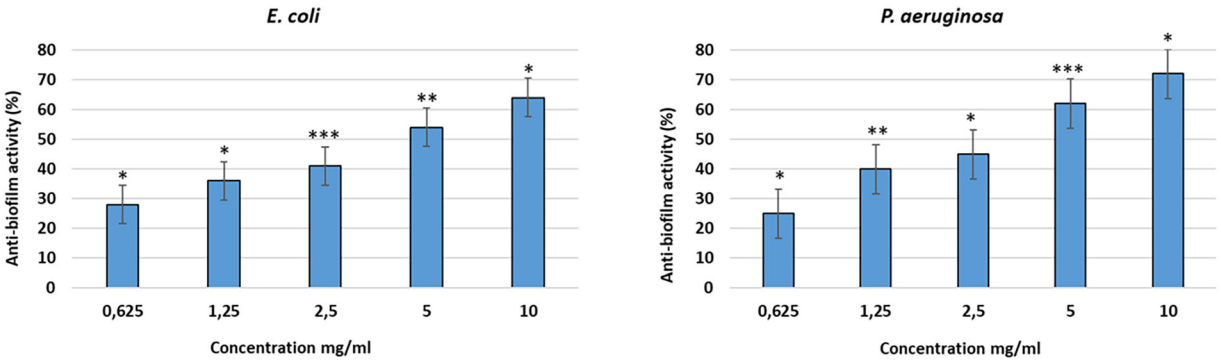

FIGURE 8 Antibiofilm activity of different concentrations of NiO nanoparticles (NPs) on the *E. coli* ATCC 25922 and *P. aeruginosa* ATCC 27853 type strains. The statistical significance values ***, ** and * denote significance at $p < 0.0001$, $p < 0.01$ and $p < 0.05$, respectively—whereas ns denotes nonsignificance.

FIGURE 9 Viability percentages of HT-22 cells after application of NiO nanoparticles (NPs) at different concentrations. The results are presented as the percentage of the control and mean ± SD. Statistical data ns: not significant, $^{**}p < 0.005$ and $^{***}p < 0.001$.

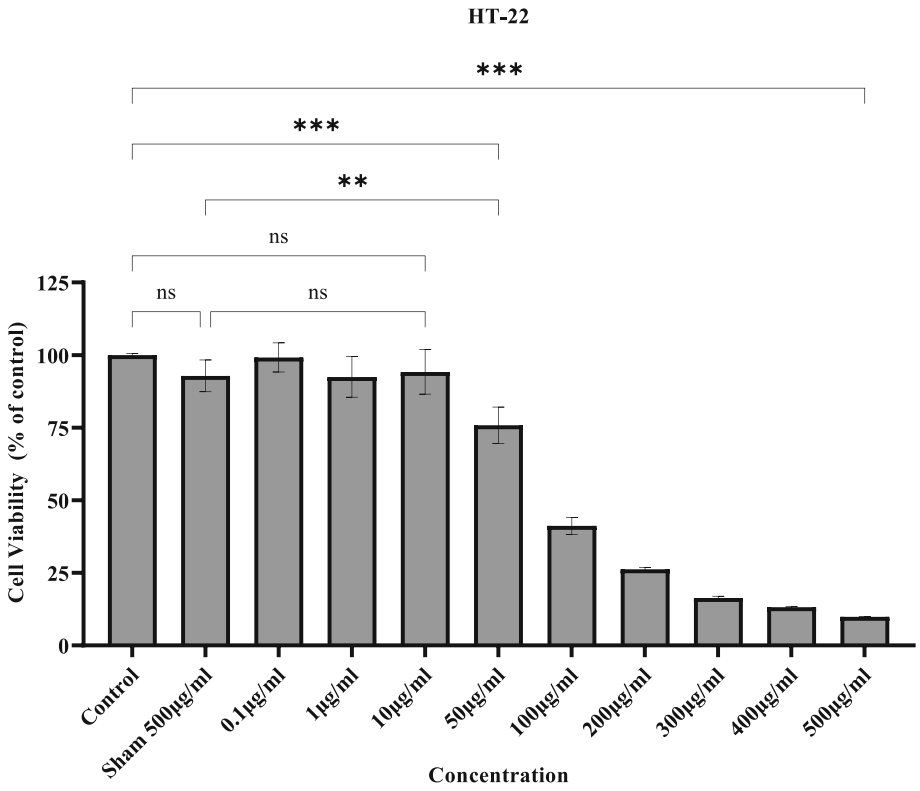

200 µg/mL NiO NPs, cell viability decreased to 66.1%, and the change in viability was determined to be significant compared with that in both the control group and the sham group ($p < 0.001$). This effect was clearly visible at this concentration. Moreover, at other concentrations, the extract had a destructive effect on MCF-7 cells, and a sudden decrease in viability of up to 17% was observed (Figure 12). For MCF-7 cells, the IC_{50} was calculated to be 206.75 ± 10.9 µg/mL.

Antimicrobial activities and minimal inhibitory concentrations were determined against *E. coli* ATCC 25922, *P. aeruginosa* ATCC 27853, *S. aureus* ATCC 25923, *B. cereus* ATCC 14579, *E. faecalis* ATCC 29212 and *S. epidermidis* ATCC 12228 bacteria using the agar well diffusion method. Additionally, antibiofilm activities were detected against the *E. coli* ATCC 25922 and *P. aeruginosa* ATCC 27853 strains that produce biofilms. The antimicrobial activities of NPs differ according to their size, synthesis conditions and strain type. Thus, the therapeutic potential of NiO NPs synthesised from Paulownia plant extract on biological and especially drug-resistant microorganisms was determined. Various researchers have previously reported the successful creation of NiO NPs using plant extracts via an environmentally friendly method.[36–39] This study indicated that the NiO particles produced have significant potential for

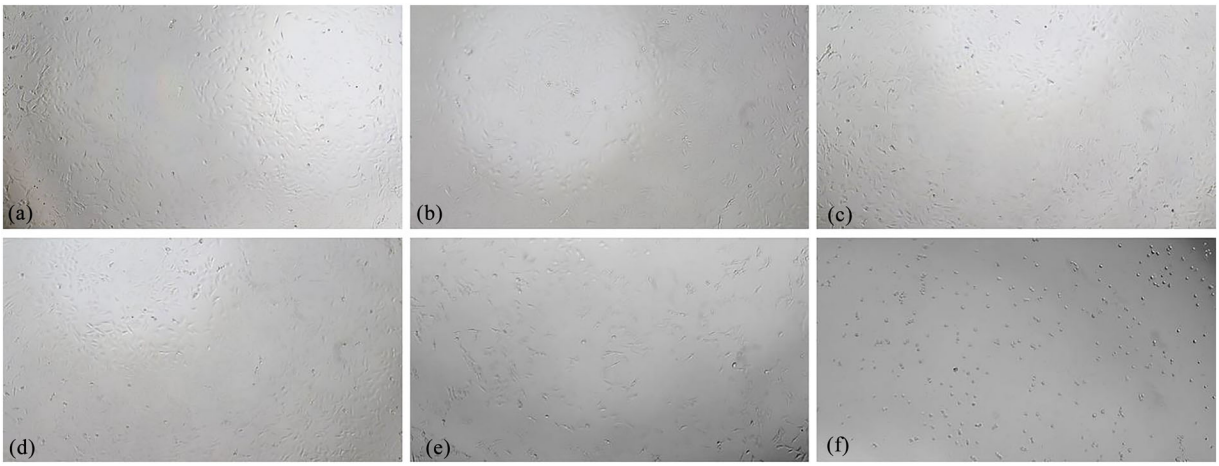

FIGURE 10 Inverted microscope images at 40× magnification after 24 h of NiO nanoparticles (NPs) application in the HT-22 cell line: (a) control, (b) 500 μg/mL sham, (c) 1 μg/mL sham, (d) 10 μg/mL sham, (e) 100 μg/mL sham and (f) 500 μg/mL sham.

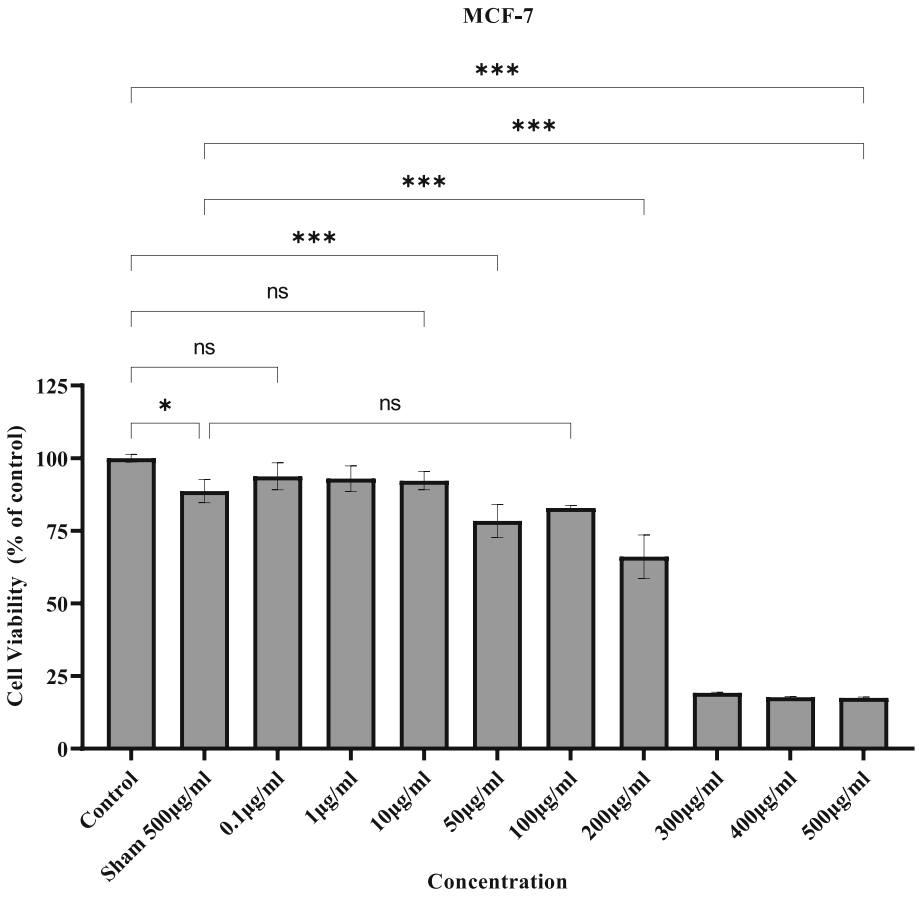

FIGURE 11 Effect of NiO nanoparticles (NPs) on the viability of MCF-7 cells. The results are presented as the percentage of the control and mean ± SD. Statistical data ns: not significant, $*p < 0.05$ and $***p < 0.001$.

antibacterial activity and can effectively combat gram-positive bacteria.[36,40]

It has been reported that factors such as metal ions released from the surface of metal NPs, which have various antimicrobial activity properties, reportedly induce the vast majority of bacteria to cause infection and antimicrobial activity.[41]

The use of plant extracts has the potential to replace traditional chemical and physical methods for NP production. In particular, plant-mediated biosynthesis has become increasingly important due to its flexibility and environmentally friendly nature. Plant extract-mediated synthesis is a rapid and straightforward process that avoids the use of toxic or unnecessary chemicals and

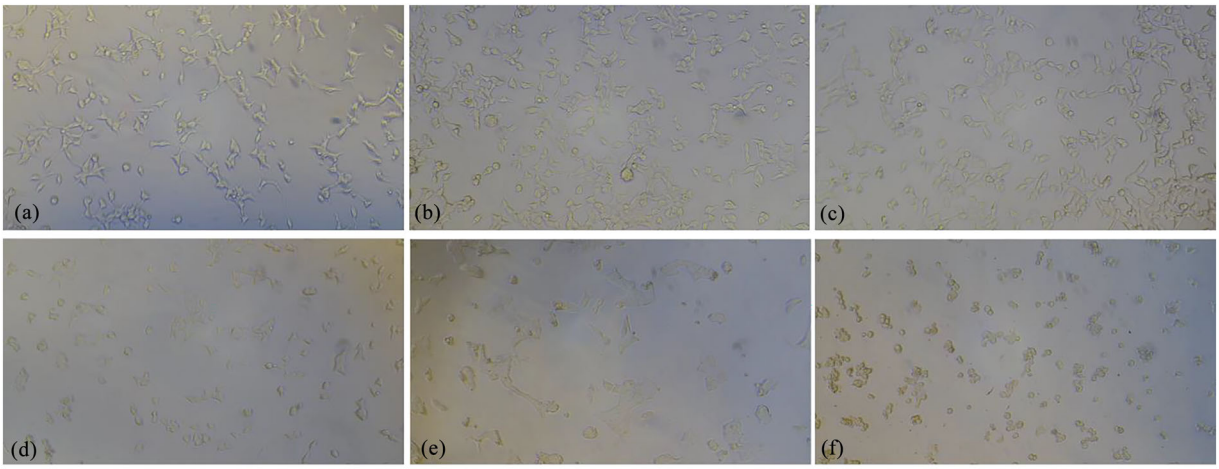

FIGURE 12 Inverted microscope images at × 100 magnification after 24 h of NiO nanoparticle (NP) application in the human breast cancer cell line: (a) control, (b) 500 μg/mL sham, (c) 1 μg/mL sham, (d) 10 μg/mL sham, (e) 100 μg/mL sham and (f) 500 μg/mL sham.

aligns with the principles of green synthesis. The presence of phytochemicals in plants is responsible for reducing metal ions during the process. The plant extract can be obtained from various parts of the plant, including the leaves, flowers, bark or seeds. In some cases, the extract is capable of reducing and stabilising the agent, as reported in a recent study.[10]

NPs are materials used to treat cancer cells due to their structure, easy conjugation with targeted biomolecules and drugs, biocompatibility and important surface modifiability.[42,43] When NPs contact cancer cells, they enter the cell and trigger oxidative stress and the formation of ROS with intracellular ion release, causing cell death. ROS formation can cause a loss of function of the mitochondrial membrane and damage cellular DNA, leading to cell apoptosis.[44] In a study conducted with NiO NPs obtained from *Areca catechu* leaf extract, the NPs were shown to have significant cytotoxic effects on a human lung cancer cell line (A549). In this study, the IC_{50} dose was 93.349 μg/mL.[45] In another study of NiO NPs obtained from *Calotropis gigantea* (a crown flower), it was reported that the NPs had significant anticancer effects on the liver cancer (HepG2) cell line.[44] In the study of NiO NPs obtained by a different method, it was stated that NiO NPs could be effective anticancer agents for three different cancer cell lines.[46]

4 | CONLUSIONS

We present first-hand reports on the development of novel, green and environmentally friendly NiO NPs from Paulownia plant extracts. NiO NPs were successfully synthesised in a green manner by a simple method at low temperature. XRD analysis revealed that the NiO NPs were in the cubical phase. The broad peak in the XRD pattern indicates the nanocrystalline behaviour of the particles. The SEM images confirmed that the NiO NPs had a spherical shape. Current study on the biological activities of NPs shows that NiO NPs have antibacterial effects. In addition, the study reveals the cytotoxic properties of NiO NPs in healthy and cancer cells. The characterisation results showed NiO NPs with a particle size of 29.64 nm. NiO NPs synthesised by green synthesis were tested against various bacteria, and the results showed antibacterial and antibiofilm effects against a broad spectrum of these materials. The results of this study highlight that Paulownia-based NiO NPs have bioactivities that may be useful as potential antibacterial agents and antibiofilms in the biomedical field. These NPs can be considered effective alternatives to standard antibiotic therapy. Green synthesis technology could pave the way for a new range of antibacterial agents.

Studies on the anti-cancer effects of NiO NPs obtained from different plant extracts on cancer cells indicate dose-dependent anti-cancer activity. However, most of these studies did not report any data on its effects on healthy cells. Our study also pointed out this deficiency and examined its effects on two groups: healthy and cancer cell lines. With our results, the NiO NPs obtained by green synthesis show a dose-dependent cytotoxic effect on the health cell line HT-22 and MCF-7 breast cancer cells. On the other hand, the IC_{50} dose value determined for the HT-22 used in the study was lower than that determined for MCF-7 cells. This suggests that when determining the anti-cancer activities of the NPs obtained, examining their effects on healthy cells and different cancer cell lines and performing detailed cellular analyses will pave the way for more accurate evaluations.

AUTHOR CONTRIBUTIONS

Güney Gürsoy: Methodology; investigation; data collection or processing; literature search and supervision. **Zehra Çiçek:** Methodology; resources; methodology; visualisation; writing—original draft. **Saniye Tekerek:** Conceptualisation; methodology; investigation; writing—original draft; writing—review and editing. **Esin Kiray:** Writing; methodology; investigation; analysis or interpretation; writing—review and editing. **Ayça Tanrıverdi:** Writing; methodology; investigation; review and editing, **Esen Çakmak:** Concept; design; methodology; investigation; writing; review and editing.

CONFLICT OF INTEREST STATEMENT

The authors declare that they have no known competing financial interests or personal relationships that could have appeared to influence the work reported in this paper.

DATA AVAILABILITY STATEMENT

The data that support the findings of this study are available on request from the corresponding author. The data are not publicly available due to privacy or ethical restrictions.

ORCID

Güney Gürsoy https://orcid.org/0000-0003-1849-9068
Zehra Çiçek https://orcid.org/0000-0003-3205-5463
Saniye Tekerek https://orcid.org/0000-0003-3326-358X
Esin Kiray https://orcid.org/0000-0002-6908-5909
Ayça Tanriverdi https://orcid.org/0000-0002-0658-8576
Esen Çakmak https://orcid.org/0000-0001-8805-3315

REFERENCES

[1] G. T. Anand, R. Nithiyavathi, R. Ramesh, S. John Sundaram, K. Kaviyarasu, *Surface Interfaces* **2020**, *18*, 100460.
[2] M. G. Berhe, Y. T. Gebreslassie, *Int. J. Nanomedicine* **2023**, *18*, 4229.
[3] S. K. Prajapati, A. Malaiya, P. Kesharwani, D. Soni, A. Jain, *Drug Chem. Toxicol.* **2022**, *45*, 435.
[4] J. Helmlinger, C. Sengstock, C. Groß-Heitfeld, C. Mayer, T. A. Schildhauer, M. Köller, M. Epple, *RSC Adv.* **2016**, *6*, 18490.
[5] Q. Yang, J. Sha, X. Ma, D. Yang, *Mater. Lett.* **2005**, *59*, 1967.
[6] R. Paulose, R. Mohan, V. Parihar, *Nano-Struct. Nano-Obj.* **2017**, *11*, 102.
[7] F. E. Ettadili, S. Aghris, F. Laghrib, A. Farahi, S. Saqrane, M. Bakasse, S. Lahrich, M. A. El Mhammedi, *J. Mol. Struct.* **2022**, *1248*, 131538.
[8] G. Kendir, A. Güvenç, *Hacettepe Univ. J. Faculty Pharm.* **2010**, *1*, 49.
[9] S. Ying, Z. Guan, P. C. Ofoegbu, P. Clubb, C. Rico, F. He, J. Hong, *Environ. Technol. Innov.* **2022**, *26*, 102336.
[10] M. Ijaz, M. Zafar, T. Iqbal, *Inorg. Nano-Metal Chem.* **2020**, *51*, 744.
[11] M. Nasrollahzadeh, S. M. Sajadi, M. Maham, *RSC Adv.* **2015**, *5*(51), 40628.
[12] S. Haq, S. Dildar, M. B. Ali, A. Mezni, A. Hedfi, M. I. Shahzad, N. Shahzad, A. Shah, *Mater. Res. Expr.* **2021**, *8*(5), 055006.
[13] M. S. Kumar, T. L. Soundarya, G. Nagaraju, G. K. Raghu, N. D. Rekha, F. A. Alharthi, B. Nirmala, *Inorg. Chim. Acta* **2021**, *515*, 120059.
[14] A. T. Khalil, M. Ovais, I. Ullah, M. Ali, Z. K. Shinwari, D. Hassan, M. Maaza, *Artif. Cells Nanomed. Biotechnol.* **2018**, *46*(4), 838.
[15] M. F. Baran, A. Baran, C. Keskin, N. Aktepe, M. N. Atalar, M. T. Adican, *Int. Target Med. J.* **2022**, *2022*(1), 10.
[16] A. Hatipoğlu, *Prog. Nutr.* **2021**, *23*, 2021242.
[17] Ö. Erdoğan, F. Birtekocak, E. Oryaşin, M. Abbak, G. M. Demirbolat, S. Paşa, Ö. Çevik, *Duzce Med. J.* **2019**, *21*(1), 19.
[18] M. G. Kang, F. Khan, D. M. Jo, D. Oh, N. Tabassum, Y. M. Kim, *Antibiotics* **2022**, *11*(11), 1524.
[19] B. Y. Öztürk, B. Y. Gürsu, İ. Dağ, *Process Biochem.* **2020**, *89*, 208.
[20] A. Kaymakci, B. C. Bal, İ. Bektas, *Kastamonu Univ. J. Forest. Faculty* **2011**, *11*, 228.
[21] P. Ji, C. Chen, Y. Hu, Z. Zhan, W. Pan, R. Li, E. Li, H. M. Ge, G. Yang, *Biol. Pharm. Bull.* **2015**, *38*, 1.
[22] J. W. Lee, K. H. Seo, H. W. Ryu, H. J. Yuk, H. A. Park, Y. R. Lim, K. S. Ahn, S. R. Oh, *J. Ethnopharmacol.* **2018**, *210*, 23.
[23] Ş. Inci, L. K. Dalkiliç, S. Kirbag, S. Dalkiliç, *Kahramanmaraş Sütçü İmam Üniversitesi Tarım Ve Doğa Dergisi* **2021**, *4*, 701.
[24] Ö. Uğuz, Y. Kara, *Int. J. Secon. Metabolite* **2019**, *6*(2), 106.
[25] U. Özge, Denizli'de Yetişen Paulownıa Tomentosa Steud'nın Fitokimyasal Profilinin Ve Elektriksel İletkenliğinin Belirlenmesi. Pamukkale Üniversitesi Fen Bilimleri Enstitüsü Biyoloji Anabilim Dalı **2018**.
[26] B. Kowalska-Krochmal, R. Dudek-Wicher, *Pathogens* **2021**, *10*, 165.
[27] M. Khan, S. Khan, M. Omar, M. Sohail, I. Ullah, *J. Chem. Rev.* **2024**, *6*(1), 94.
[28] F. Liu, X. Wang, J. Hao, S. Han, J. Lian, Q. Jiang, *Sci. Rep.* **2017**, *7*(1), 17709.
[29] A. A. Neamah, A. M. N. Khaleel, *Chem. Methodol.* **2022**, *6*(5), 372.
[30] A. Rahdar, M. Aliahmad, Y. Azizi, *J. Nanostructure* **2015**, *5*(2), 145.
[31] F. Hakimi, F. S. Oreyzi, F. Bani Fatemeh, E. Golrasan, *Asian J. Green Chem.* **2020**, *4*(2), 134.
[32] J. F. Li, B. Xiao, L. J. Du, R. Yan, T. D. Liang, *J. Fuel Chem. Technol.* **2008**, *36*, 42.
[33] M. Srivastava, S. Chaubey, A. K. Ojha, *Mater. Chem. Phys.* **2009**, *118*, 174.
[34] J. Sachin, N. Singh, R. Singh, K. Shah, B. K. Pramanik, *Chemosphere* **2023**, *327*, 138497.
[35] M. Hafeez, R. Shaheen, B. Akram, M. N. Ahmed, Z. Abdin, S. Haq, S. Ud Din, M. Zeb, M. A. Khan, *S. Afr. J. Chem.* **2021**, *75*, 168.
[36] A. A. Ezhilarasi, J. J. Vijaya, K. Kaviyarasu, M. Maaza, A. Ayeshamariam, L. J. Kennedy, *J. Photochem. Photobiol. B* **2016**, *164*, 352.
[37] B. T. Sone, X. G. Fuku, M. Maaza, *Int. J. Electrochem. Sci.* **2016**, *11*, 8204.

[38] F. T. Thema, E. Manikandan, A. Gurib-Fakim, M. Maaza, *J. Alloys Compd.* **2016**, *657*, 655.
[39] M. A. Nasseri, F. Ahrari, B. Zakerinasab, *Appl. Organomet. Chem.* **2016**, *30*, 978.
[40] H. E. Rani, *Int. J. Sci. Res.* **2015**, *4*(11), 216.
[41] Y. Saygılı, F. Ünal, D. Yüzbaşıoğlu, *Int. J. Adv. Eng. Pure Sci.* **2021**, *33*, 429.
[42] M. Nikzamir, A. Akbarzadeh, Y. Panahi, *J. Drug Deliv. Sci. Technol.* **2021**, *61*, 102316.
[43] M. Vairavel, E. Devaraj, R. Shanmugam, *Environ. Sci. Pollut. Res.* **2020**, *27*, 8166.
[44] N. Venkatalakshmi, H. Jyothi Kini, H. S. Bhojya Naik, *Inorg. Chem. Commun.* **2023**, *151*, 110490.
[45] U. R. Shwetha, C. R. Rajith Kumar, M. S. Kirani, S. B. Virupaxappa, M. S. Latha, V. Ravindra, G. Lamraoui, A. A. Al-Kheraif, A. A. Elgorban, A. Sayed, S. Chandan, S. P. Kollur, *Molecules* **2021**, *26*, 2448.
[46] M. A. J. Kouhbanani, Y. Sadeghipour, M. Sarani, E. Sefidgar, S. Ilkhani, A. M. Amani, N. Beheshtkhoo, *Green Chem. Lett. Rev.* **2021**, *14*(3), 444.

How to cite this article: G. Gürsoy, Z. Çiçek, S. Tekerek, E. Kiray, A. Tanriverdi, E. Çakmak, *Appl Organomet Chem* **2024**, *38*(6), e7492. https://doi.org/10.1002/aoc.7492